On the Performance of mmWave Networks aided by Wirelessly Powered Relays

On the Performance of mmWave Networks aided by Wirelessly Powered Relays

Sudip Biswas, *Student Member, IEEE*, Satyanarayana Vuppala, *Member, IEEE*
and Tharmalingam Ratnarajah, *Senior Member, IEEE*

***Abstract*—We investigate the energy harvesting (EH) potential of an outdoor millimeter-wave (mmWave) network aided by wirelessly powered relays (WRs). Due to the effect of propagation characteristics, such as blockages, WRs can assist the coverage in mmWave networks. In this paper, we consider the WRs to be equipped with battery units that can store ambient RF energy from the mmWave sources. The sources and the WRs are modeled as independent homogeneous Poisson point processes (PPPs). Leveraging tools from stochastic geometry, we study the EH potential of the WRs and their coverage probability based on the amount of energy that can be harvested. To successfully receive and transmit, the batteries in the WRs have to store sufficient energy, while the received signal to interference plus noise (SINR) ratio at the destination is above a certain threshold level. We also analyze the node isolation and network connectivity probabilities for the WRs considering a bounded region. Based on this bounded region of the WRs, we then select the best WR to forward the message from sources to the destination. Furthermore, the coverage probability is also analyzed for the WRs residing both within and outside the bounded region.**

***Index Terms*—Energy Harvesting, mmWave Networks, Poisson Point Processes, Wireless Relay, Stochastic Geometry.**

I. Introduction

The fifth generation (5G) wireless communication systems are being developed to meet the exponential growth in mobile data traffic. The key goals include data rates in the range of Gbps, billions of connected devices, lower latency, improved coverage and reliability and low-cost, energy efficient and environment-friendly operation. Moreover, keeping in mind that the current wireless spectrum is almost saturated, it is imperative to shift the paradigm of cellular spectrum to a new range of frequencies. In this regard, millimeter wave (mmWave) bands with significant amounts of unused or moderately used bandwidths are being considered as a suitable alternative to the current microwave spectrum. The availability of bands in the range of 20-100 GHz makes mmWave a lucrative prospect in the design of 5G networks.

Massive MIMO, which is another technology that is being considered for 5G can be implemented through mmWave systems, as such systems will require large dimensional antenna arrays to perform directional beamforming at the transmitter/receiver. In [1] it was stated that very large antenna arrays may not be useful when the antennas are deployed within a fixed physical space. However, the smaller wavelengths of mmWave bands will make it possible to rig a large number of antennas in constrained physical spaces. Furthermore, to increase the coverage probability of mmWave systems and make it somewhat comparable to microwave systems, it is mandatory to deploy the base stations (BSs) densely [2]. In [3], the authors explore mmWave frequency bands to design a 5G enhanced Local Area Network (eLAN). While [4] proposes a general framework to analyze the coverage and rate performance of mmWave networks, [5] proposes a tractable mmWave cellular network model and analyzes the coverage rate. These design features of mmWave makes encourages radio frequency (RF) energy harvesting (EH), where a node may harvest the ambient mmWave energy incident on it. A receiver architecture for mmWave systems was proposed in [6] for simultaneous wireless information and power transfer. EH solutions to power devices have been studied in literature for quite a while, with moderate level of practical success [7]. The recent outburst of low powered internet of things (IoT) can potentially take advantage of EH in the future.

However, mmWave cellular communication is heavily dependent on the propagation environment and is affected by several environmental factors such as atmospheric conditions and physical obstacles like buildings, concrete walls, vehicles, trees etc. Recent studies and measurements however have revealed that the significant increase in omnidirectional path loss can be compensated by the proportional increase in overall antenna gain with appropriate beamforming. The performance of mmWave cellular systems was analyzed in [8] using real time propagation channel measurements. Blockage effects and angle spreads were also incorporated in [9] to analyze mmWave systems. Generally in a communication system, path losses are computed for both line-of-sight (LOS) and non-line-of-sight (NLOS) measurements. It was stated in [10] that the blockages cause substantial differences in the LOS and NLOS path loss characteristics. Considering the cons of mmWave systems, it is not clear if such a technology will be suitable for energy harvesting, which is why we intend to analyze the performance of such systems taking energy harvesting into consideration.

In conventional communication systems, relay aided transmission has been regarded as an effective way to increase the coverage probability, throughput and transmission reliability of the networks [11]. While [12] considers the deployment of relays as a network infrastructure without a wired backhaul connection, [13] explores the potential of deploying relays to design a cost effective network. It was shown in [14] that the use of relays can be a promising solution for mmWave systems to combat the blockage effects and path losses that are encountered in mmWave networks. In this regard, multiple

This work was supported by the UK Engineering and Physical Sciences Research Council (EPSRC) under grant number EP/L025299/1.

S. Biswas, S. Vuppala and T. Ratnarajah are with the Institute for Digital Communications, the University of Edinburgh, King's Building, Edinburgh, UK, EH9 3JL. E-mails: [Sudip.Biswas; S.Vuppala; T.Ratnarajah]@ed.ac.uk. Correspondent author: S. Vuppala.

relays can be deployed between the sources and the destination of a transmission link. Performance evaluation of relay aided networks has been widely studied in [15], [16]. In [17], authors have studied the coverage probability of relay aided cellular networks with different association criteria between the base station and mobile station. It has been shown that coverage probability highly depends on path loss exponents and density of relays. Similarly, the achievable transmission capacity has been analyzed in relay assisted device-to-device networks in [18]. The performance of Decode-and-Forward and Amplify-and-Forward strategies with high gain antenna arrays was characterized in [19]. The numerical results proved that directional antennas are useful for multi-hop relays. Hence, it is implicit that relays can prove to be an important tool in the design of mmWave cellular systems because coverage in such systems is a more acute problem, given the large difference between LOS and NLOS propagation characteristics.

A relay spends its own energy while forwarding the information from a source to the destination. Physical cables supply power to the relay nodes, which is cumbersome and unmanageable in most circumstances. A common solution to this is to supply power to the relay with a pre-charged battery. However, the battery drains out proportionally to the use of the relay and after the battery is completely exhausted, the relay can no longer assist in transmission. Some useful techniques have been presented in literature such as fairness mechanisms [20] and network lifetime maximization techniques [21], which help alleviate the issue. However, we cannot escape the fact that relays will still eventually run out of power. In this regard, the use of EH nodes as relays can be an alluring solution. These relay nodes can harvest energy from the ambient RF available in the atmosphere in order to perform the signal processing and communication tasks. EH relays can ensure a enduring network operation without the need for replacing the batteries frequently as, when the relay node drains its battery, it can harvest energy and recharge its own battery to aid the communication again.

Recently, stochastic geometry approaches have been widely used to develop tractable models for the performance evaluation of wireless networks [22]. In this approach, the wireless network is abstracted to a convenient point process that is used to capture the network properties. A poisson point process (PPP) is the most popular and tractable point process to model the locations of users and base stations in wireless networks. [23] models the base stations as a PPP and determines the aggregate coverage probability. Inspired by the stochastic geometry approach to analyze the performance of conventional cellular systems, we design a framework to characterize the wireless power and information transfer in mmWave networks aided by relays. However, applying the results of conventional cellular systems to mmWave is non-trivial due to their differences in propagation characteristics and the use of highly directional beamforming. Directional beamforming was applied in [24] by considering a simplified path loss model. While in [25] a blockage model for mmWave is used to analyze the rate and coverage area of such systems, a distance dependent path loss model is considered along with antenna gain parameters in [5] to characterize the propagation environment in mmWave systems. Furthermore, we would like to refer the readers to [3]–[5], [25] which develop several mathematical frameworks to model the propagation characteristics of mmWave networks.

Understanding the performance benefits of using wireless relays (WRs), that can harvest energy wirelessly in mmWave networks is thus, an important and challenging problem, which is the focus of this paper. We incorporate WRs to aid mmWave networks in order to provide better coverage and decrease blockage effects on the transmission link. Moreover, in our model, we will use EH decode-and-forward (DF) relays, because such relays are well investigated in literature [26], [27] and are considered to be suitable for low complexity wireless nodes. We assume that the EH process is stationary and ergodic and WR nodes take part in the information transfer if and only if they have enough energy to transmit the data. We consider a stochastic geometry approach to characterize the spatially distributed WRs and sources. It is assumed that the sources and the WRs in the mmWave network follow two PPPs but are independent of each other. We consider the WR nodes to be distributed according to Matern hard-core point process (MHCPP). Due to the fact that some WRs are not in operation owing to their incapability to harvest enough energy, we consider the subset of relays which has accumulated enough power to assist the transmission. This consideration leads to a marked Poisson process. After analyzing the harvested power in the WRs, we focus on the coverage probability and transmission capacity of the WRs. To gain further insight, we study the impact of interference during the transmission from the WRs to the destination by evaluating the WR node isolation probability.

In particular, our work can be divided into two parts- a) Energy Harvesting and b) Performance analysis. For the case of EH, we approximate the aggregate harvested energy as a gamma random variable and characterize it using two approaches, namely Laplace characterization and cumulant characterization. Later, to analyze the performance of our model, we introduce two metrics namely, node isolation probability and network connectivity. Our analysis provides insights on the future and benefits of wirelessly powered relay nodes with respect to the soon to be implemented mmWave communication. We also provide a detailed analysis on the effect of path loss coefficient, node density, and signal-to-interference-plus-noise ratio (SINR) threshold on a WR aided mmWave network.

Notations: We use upper and lower case to denote cumulative distribution functions (CDFs) and probability density functions (PDFs) respectively. $\mathbb{R}$ denotes the real plane while $\mathbb{Z}^+$ denotes the plane for real and positive integers. The probability is denoted by $\mathbb{P}[\cdot]$ and expectation by $\mathbb{E}[\cdot]$. All other symbols will be explicitly defined wherever used.

The rest of the paper is organized as follows. Section II describes the system model. The battery modeling and analysis of the harvested energy are presented in Section III and in Section IV, we analyze the system with respect to various performance metrics including the node isolation probability and node connectivity. Section V gives the simulation results followed by the conclusion in Section VI.

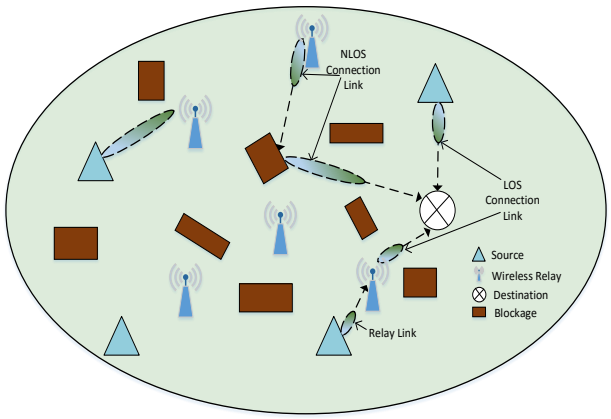

Fig. 1: An illustration of an outdoor mmWave network setup aided by wirelessly powered relays.

II. System Model

In this section, we illustrate our system model of an outdoor mmWave ad hoc network consisting of multiple sources transmitting to a typical destination (reference point) aided by WRs as shown in Fig. 1. The destination is assumed to be located at the origin $\mathcal{O}$. We term the direct link between a source and the destination or a WR and the destination as connection link. The link between a source and a WR is termed as the relay link. The sources in the network are modeled as points in $\mathbb{R}^2$ which are distributed uniformly as a homogeneous PPP Φ_{S} with intensity λ_{S}. The WRs are also modeled as points of a uniform PPP, denoted by Φ_{R}, with density λ_{R} in $\mathbb{R}^2$. The WRs are powered wirelessly by harvesting energy during the downlink transmission from the sources to the WRs. For analytical tractability, we consider that all the sources transmit with the same power P_{S} during downlink transmission from sources to the WRs and the destination.

In mmWave networks, small scale fading does not have as much impact on transmitted signals as compared to lower frequency systems. However, blockages and shadowing are more significant in such systems. It is extensively mentioned in [3], [9] that in mmWave analysis, small scale fading can be ignored. However, to capture a generalised propagation environment, we consider the Nakagami fading model.

Now, considering the Nakagami-m channel model [28], the channel power is distributed according to

$$\mathcal{X} \sim f_{\mathcal{X}}(x;m) \triangleq \frac{m^m x^{m-1} e^{-mx}}{\Gamma(m)}, \tag{1}$$

where m is the Nakagami fading parameter and $\Gamma(m)$ is the upper incomplete gamma function. In the following, we elaborate on a few other parameters that characterize our mmWave system model.

1) Directional beamforming modeling: Due to the small wavelength of mmWaves, directional beamforming can be exploited for compensating the path loss and additional noise. Accordingly, antenna arrays are deployed at the transmitter and receiver pairs. In our model, we assume all the transmit and receiver pairs to be equipped with directional antennas with sectorized gain pattern. Let θ be the beamwidth of the main lobe. Then the antenna gain pattern for a source, WR or destination node about some angle ϕ is given as [4]

$$G_q(\theta) = \left\{ \begin{array}{ll} G_q^{\max} & \text{if} |\phi| \leq \theta \\ G_q^{\min} & \text{if} |\phi| \geq \theta \end{array} \right\}, \tag{2}$$

where $q \in \mathrm{S}, \mathrm{R}, \mathrm{D}$, $\phi \in [0, 2\pi)$ is the angle of boresight direction, $G_q^{(max)}$ and $G_q^{(min)}$ are the array gains of main and side lobes, respectively. Hereinafter, for simplicity we assume the antenna beams of the connection link and the relay link to be aligned. Hence, the total gain on any desired link is $G^{\max}$.

2) Blockage modeling: Blockages in the network are usually concrete buildings which cannot be penetrated by mmWaves. We consider the blockages to be stationary blocks which are invariant with respect to direction. Leveraging the modeling of blockage in [29], we consider a two state statistical model for each and every link. The link can be either LOS or NLOS. LOS link occurs when there is a direct propagation path between the transmitter and the receiver, while NLOS occurs when the link is blocked and the receiver receives the signal through reflection from a blockage. Let the LOS link be of length r, then the probabilities of occurrence $p_{\mathrm{L}}(.)$ and $p_{\mathrm{N}}(.)$ of LOS and NLOS states respectively can be given as a function of r as

$$p_{\mathrm{L}}(r) = e^{-\beta r}, \quad p_{\mathrm{N}}(r) = 1 - e^{-\beta r}, \tag{3}$$

where β is the blockage density.

Another model that has been considered in literature is a fixed LOS probability model, as was depicted in [5]. Let the LOS area within a circular ball of radius r_D be centered around the reference point. Then, if the LOS link is of length r, the probability of the connection link to be LOS is given by p_{L} if $r < r_D$ and 0 otherwise. The parameters r and r_D are dependent on the geographical and deployment scenario of the network. Our results are based on the data from [5]. Henceforth, all notations with subscripts L and N will correspond to their respective LOS and NLOS parameters.

3) SINR modeling: In order to characterize the SINR distribution, we assume a two slot synchronous communication throughout the paper. In the first time slot, the source transmits to the WRs and the destination while in the second time slot, one of the WRs decode and forwards the signal it has received to the typical destination. It is possible that due to the EH nature of the WRs, no WR is available in the second time slot. At the end of the second time slot, the destination optimally combines the signals it has received in the two time slots.

First Time Slot: Consider that the WR nodes are served by the sources during this time slot. By a slight abuse of notation, we consider Φ_{S} to be the set of interfering sources. The SINR at any specific WR, R can then be formulated as

$$\gamma_{\mathrm{SR}_l} \triangleq \frac{P_{\mathrm{S}} G_l^{\max} |h_{\mathrm{SR}_l}|^2 r_{\mathrm{SR}_l}^{-\alpha_j}}{\sigma_{\mathrm{SR}}^2 + \sum\limits_{i \in \Phi_{\mathrm{S}}} P_{\mathrm{S}} G_i^{\max} |h_{\mathrm{SR}_i}|^2 r_{\mathrm{SR}_i}^{-\alpha_j}}, \tag{4}$$

where $P_{\rm S}$ is the transmit power of the source, $r_{{\rm SR}_l}$[1] is the length of the link from the source to WR, $h_{{\rm SR}_l}$ is the fading gain at the WR of interest, α_j is the path loss exponent with $j \in \{\rm L,\ N\}$, $\sigma^2_{\rm SR}$ is the noise power, $h_{{\rm SR}_i}$ denotes each interference fading gain and $r_{{\rm SR}_i}$ is the distance from the interferer i to the typical receiver.

Now, consider that the destination, D is served by a source during this time slot. Then the SINR at the destination D receiving signal only from the source S can be given as

$$\gamma_{{\rm SD}_l} \triangleq \frac{P_{\rm S} G_l^{\max} |h_{{\rm SD}_l}|^2 r_{{\rm SD}_l}^{-\alpha_j}}{\sigma^2_{\rm SD} + \sum\limits_{i \in \Phi_{\rm S}} P_{\rm S} G_i^{\max} |h_{{\rm SD}_i}|^2 r_{{\rm SD}_i}^{-\alpha_j}}. \tag{5}$$

Second Time Slot: Similarly, by a slight abuse of notation, we consider $\Phi_{\rm R}$ to be the set of interfering WRs. The SINR at the destination D receiving signal only from the WR R can then be given as

$$\gamma_{{\rm RD}_l} \triangleq \frac{\rho G_l^{\max} |h_{{\rm RD}_l}|^2 r_{{\rm RD}_l}^{-\alpha_j}}{\sigma^2_{\rm RD} + \sum\limits_{i \in \Phi_{\rm R}} \rho G_i^{\max} |h_{{\rm RD}_i}|^2 r_{{\rm RD}_i}^{-\alpha_j}}. \tag{6}$$

where ρ is the minimum power required for transmission through the WR.

Now, considering that the source transmits to the destination only through the aid of the WR, the coverage probability of such a WR-aided transmission link with a target SINR, T is given by

$$\mathcal{P}^c_{\rm R} = 1 - \mathbb{P}\{\gamma_{{\rm SR}_l} < T\}\mathbb{P}\{\gamma_{{\rm RD}_l} < T\}. \tag{7}$$

III. Energy Harvesting

In the context of the analysis in the paper, we assume that the power supply for the WRs are confided to the energy harvested from ambient mmWave radio frequency (RF) energy sources only. In this section, we elaborate on the modeling of the battery of the WRs and the corresponding EH analysis.

A. WR Battery Modeling

An illustration of a wirelessly powered relay is shown in Fig. 2. The WR stores the harvested energy in its battery, and then draws power from it. For analytical tractability, we assume the battery capacity to be unbounded. The WRs use the harvested energy to forward the information from sources to the destination. It is to be noted that the energy is harvested at the WR from the sources during the transmission link $r_{\rm SR}$. The energy harvested by a WR over time is assumed to be a stationary and ergodic. We also assume that the transfer of information and power do not take place simultaneously. In other words, all the antennas in a WR will either harvest energy or receive information from the sources or will forward the information to the destination. Accordingly, the WRs will harvest energy from the sources during the transmission link and store this energy in their respective batteries. This process

[1] $r_{\rm AB}$ is the distance between the A-th and B-th nodes.

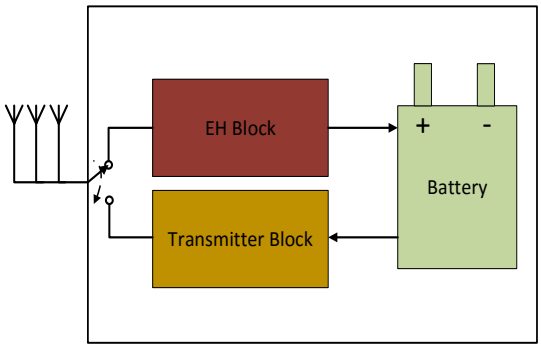

Fig. 2: Topology of an EH WR consisting of EH, transmitter and battery blocks.

continues for a particular WR until it harvests enough energy to receive and forward the information to the destination with the aid of the harvested power from its battery. The model considered in our paper encompasses several energy profiles assumed in literature. For example, while in [7], energy is harvested with a specific probability in every time slot, a Markov model was used in [30]. All the WRs are assumed to be equipped with a EH circuit, which converts the mmWave RF power into DC power with a conversion efficiency of $\xi \leq 1$. The aggregate harvested power by any WR node can be looked upon as the sum of independent positive random variables $P_{\rm S} G_i^{\max}) h_{{\rm SR}_i^j} ||r_{{\rm SR}_i^j}||^{-\alpha_j}$, with $i = 1 \ldots K$ being nodes in $\Phi_{\rm S}$. Accordingly, the EH power can be given as

$$P_{\mathbb{H}_j} = \xi \sum_{i=1}^{K} P_{\rm S} G_i^{\max} h_{{\rm SR}_i} ||r_{{\rm SR}_i}||^{-\alpha_j}, \tag{8}$$

where $j \in \{\rm L,\ N\}$.

In the subsequent analysis, we analyze this EH power with respect to its CDF and PDF in order to attain insights on the performance of the WR nodes in a mmWave network.

B. Laplace Characterization of Harvested Power

To obtain the PDF of the harvested power, one must obtain the Laplace transform of (8) followed by its inverse Laplace transform. As discussed before, we will consider two blockage probability models from literature as follows.

1) Exponential blockage probability model: This blockage modeling follows from section II. Below we give propositions which characterize the Laplace transform of the EH power of a WR with respect to this model.

Proposition 1. *The Laplace transform of the EH power of a WR node in a mmWave network, considering the exponential blockage probability model is given by*

$$\mathcal{L}\{P_{\mathbb{H}_j}\}(s) = \tag{9}$$
$$\prod_j \exp\left[-2\pi\lambda_{\rm S} \int_1^\infty \left(1 - \frac{1}{1 + \frac{s\,\xi\,P_{\rm S} G_i^{\max}}{m} r^{-\alpha_j}}\right)^m r p_j(r) dr\right],$$

where p_j is the exponential blockage probability, which follows from (3).

Proof. Consider the LOS case, where $p_{\rm L}(r) = e^{-\beta r}$. Now taking the Laplace transform of (8) we have

$$\mathcal{L}\{P_{\mathbb{H}_j}\}(s) = \mathbb{E}[\exp(-sP_{\mathbb{H}_j})],$$
$$\overset{(a)}{=} \mathbb{E}_{\Phi_{\rm S}}\left\{\prod_{i\in\Phi_{\rm S}} \mathbb{E}_{h_{{\rm SR}_i}}\left[\exp\left(-s\,\xi P_{\rm S} G_i^{\max} h_{{\rm SR}_i}||r_{{\rm SR}_i}||^{-\alpha_j}\right)\right]\right\}, \tag{10}$$
$$\overset{(b)}{=} \mathbb{E}_{\Phi_{\rm S}}\left\{\prod_{i\in\Phi_{\rm S}} \left(\frac{1}{1+\frac{s\,\xi\,P_{\rm S}G_i^{\max}}{m} r^{-\alpha_j}}\right)^m\right\}, \tag{11}$$
$$\overset{(c)}{=} \exp\left[-2\pi\int_1^\infty \left(1-\frac{1}{1+\frac{s\,\xi\,P_{\rm S}G_i^{\max}}{m} r^{-\alpha_j}}\right)^m e^{-\beta r}{\rm d}r\right], \tag{12}$$

where (a) follows from the assumption of independent small scale fading, (b) follows from the use of the moment generating function of exponentially-distributed random variables and (c) follows due to the use of probability generating functionals of PPPs. The NLOS case is obtained similarly. □

In order to simplify the Laplace transform, in the subsequent sub-section we consider the fixed blockage model for mmWave systems.

2) Fixed blockage probability model: We note that the adoption of fixed LOS probability model in our analysis simplifies expressions for the evaluation of the numerical integrals. It has been shown via simulations in [14] that the error due to such an approximation (LOS step model) is generally small in dense mmWave networks, which also motivates the use of this first-order approximation of the LOS probability function which simplifies the dense network analysis. As shown in [14, Fig. 9], the step function approximation generally provides a lower bound of the actual SINR distribution, and the errors due to the approximation become smaller when the base station density increases. Accordingly, considering the fixed blockage probability model, the Laplace transform of (8) is given in the following proposition.

Proposition 2. *Let, $\Xi = \frac{\xi P_{\rm S} G_i^{\max}}{m}$. Then, considering the fixed blockage probability model, the Laplace transform of EH power of a WR node in a mmWave network is given by*

$$\mathcal{L}\{P_{\mathbb{H}_j}\}(s) = \tag{13}$$
$$\prod_j \exp\left(-2\pi\lambda_{\rm S}\left\{(s\Xi)^{\frac{2}{\alpha_j}-1}\mathbb{B}\left[\frac{-1}{\Xi\,s}, \frac{2}{\alpha_j}-i+m, 1-m\right]\right.\right.$$
$$\left.\left. -\,(s\,\Xi)^{-m}\,\alpha_j\,2\mathbb{F}_1\left[m, \frac{2}{\alpha_j}+m, 1+\frac{2}{\alpha_j}+m, \frac{-1}{\Xi\,s}\right]\right\}\right),$$

where $\mathbb{B}$ is the Beta function and $2\mathbb{F}$ is a hypergeometric function.

Proof. Consider the LOS case, and a fixed blockage probability $p_{\rm L}$. Now taking the Laplace transform of (8) we have

$$\mathcal{L}\{P_{\mathbb{H}_j}\}(s) = \exp\left[-2\pi\lambda_{\rm S}\int_1^\infty\left(1-\frac{1}{(1+\Xi\,s r^{-\alpha_j})^m}\right) r\,p_{\rm L}{\rm d}r\right],$$
$$= \exp\left[-2\pi\lambda_{\rm S}\int_0^\infty \frac{(1+\Xi\,s\,r^{-\alpha_j})^m - 1}{(1+\Xi\,s\,r^{-\alpha_j})^m} r\,p_{\rm L}{\rm d}r\right],$$
$$= \exp\left[-2\pi\lambda_{\rm S}\underbrace{\int_0^\infty\left(\frac{\sum_{i=0}^m(-1)^i\binom{m}{i}}{(1+\Xi\,s\,r^{-\alpha_j})^m}\right) r\,p_{\rm L}{\rm d}r}_{I_1}\right.$$
$$\left. -\underbrace{\int_0^\infty \frac{1}{(1+\Xi\,s\,r^{-\alpha_j})^m} r\,p_{\rm L}{\rm d}r}_{I_2}\right].$$

By change of variables ($z = r^{-\alpha_j}$), we now have

$$I_1 = \sum_{i=0}^m \frac{\binom{m}{i}(-1)^{i+1}p_{\rm L}}{\alpha_j}\int_0^\infty\left(\frac{z^{i-1-\frac{2}{\alpha_j}}}{(1+\Xi\,s\,z)^m}\right){\rm d}z,$$
$$= (s\Xi)^{\frac{2}{\alpha_j}-1}\,\mathbb{B}\left[\frac{-1}{\Xi\,s}, \frac{2}{\alpha_j}-i+m, 1-m\right], \tag{14}$$

$$I_2 = p_{\rm L}\int_0^\infty\left(\frac{z^{\frac{-1}{\alpha_j}}}{(1+\Xi\,s\,z)^m}\frac{1}{z^{1+\frac{1}{\alpha_j}}}\right){\rm d}z,$$
$$= (\Xi s)^{-m}\,\alpha_j\,2\mathbb{F}_1\left[m, \frac{2}{\alpha_j}+m, 1+\frac{2}{\alpha_j}+m, \frac{-1}{\Xi\,s}\right]. \tag{15}$$

Plugging I_1 and I_2 into (14), we obtain the required proof. The NLOS case also follows similarly by replacing the blockage probability with $1-p_{\rm L}$. □

At this point it is worthwhile to mention that the Laplace transform of EH power doesn't actually admit closed form expressions under either the exponential blockage model or the fixed blockage model. Hence, for analytical tractability, in the next sub-section we will use the cumulant approach to approximate the distribution of the harvested power. However, it is possible to obtain a closed form solution for only the NLOS case under fixed blockage model, as can be seen from the following corollary.

Corollary 1. *For the NLOS case, considering Rayleigh fading and the fixed blockage probability model, the Laplace transform for the EH power of a WR node can be given as*

$$\mathcal{L}\{P_{\mathbb{H}_{\rm N}}\}(s) = \exp\left(-2\pi^2\lambda_{\rm S}\frac{(1-p_{\rm L})(s\xi P_{\rm S}G_i^{\max})^{\frac{2}{\alpha_{\rm N}}}}{\alpha_{\rm N}\sin(\frac{2\pi}{\alpha_{\rm N}})}\right). \tag{16}$$

C. Cumulant characterization of Harvested Power

In this section, we characterize the EH power through cumulants of the probability distribution. This approach is an alternative to the above analysis, which has been used extensively in probability theory and statistics. We note that

the number of terms K in (8) is a Poisson random variable, which is assumed to be independent of the summands. Since $P_{\mathbb{H}_j}$ is the sum of independent positive random variables, it is a Poisson compound sum. Based on the distribution of the summands, a closed-form expression for the distribution of the Poisson compound sum may be obtained as [31]. However, calculating the tail probability of the Poisson compound sum is not a trivial process, and several approximation techniques have been studied in literature. One of the approximation techniques is the use of Gamma-type analytical distributions. The Gamma-type analytical distribution, along with other distributions like the mixed-gamma and the shifted-gamma distributions have been successfully used to approximate distribution of Poisson sums [32]. Here, we adopt the Gamma distribution to approximate the distribution of the compound Poisson sum of EH power of a WR. Hence, in order to parameterize the distribution, we adopt the cumulant approach in the following analysis.

Let $\mathcal{X} \triangleq |h_{\mathrm{SR}}|^2$. Hence, under the consideration of this model and the use of Campbell's theorem, the characteristic function of $P_{\mathbb{H}_j}$ can be computed by [33] as

$$\mathcal{W}\{P_{\mathbb{H}_j}\}(s) = \exp\left(-2\pi\lambda_{\mathrm{S}} \int_{h_{\mathrm{SR}}} \int_{\mathbb{R}^2} [1 - e^{isxr^{-\alpha_j}}] f_{\mathcal{X}}(x)\, \mathrm{d}r\mathrm{d}x\right), \quad (17)$$

where i is the imaginary unit.

Now, for the LOS case, the n-th cumulant of $\mathcal{L}\{P_{\mathbb{H}_{\mathrm{L}}}\}(s)$ can be given by

$$\kappa(n) = \frac{1}{i^n} \frac{\mathrm{d}^n \log(\mathcal{W}\{P_{\mathbb{H}_{\mathrm{L}}}\}(s))}{\mathrm{d}s^n}\Big|_{s=0} \quad (18)$$

$$\begin{aligned}\kappa(n) &= 2\pi\lambda \int_{\mathcal{X}} \int_1^{\infty} \left[x^n r^{1-n\alpha_{\mathrm{L}}} f_{\mathcal{X}}(x) e^{-\beta r}\right. \\ &\qquad \left. + x^n r^{1-n\alpha_{\mathrm{N}}} f_{\mathcal{X}}(x)(1 - e^{-\beta r})\right] \mathrm{d}r\mathrm{d}x, \\ &= 2\pi\lambda_{\mathrm{S}} \mathbb{E}[\mathcal{X}^n] \left[\mathrm{EI}[(n\alpha_{\mathrm{L}} - 1)\beta]\right. \\ &\qquad \left. + \tfrac{1}{n\alpha_{\mathrm{N}} - 1} - \mathrm{EI}[(n\alpha_{\mathrm{N}} - 1)\beta]\right], \end{aligned} \quad (19)$$

where EI denotes the exponential integral. The closed form expressions of $\kappa(n)$ under Gamma distributions are also provided in [33].

Accordingly, we obtain the following parameters of Gamma distribution,

$$f^{(\Gamma)}(x; \nu, \theta) = \frac{x^{\nu-1} e^{-\frac{x}{\theta}}}{\theta^{\nu} \Gamma(\nu)}, \quad (20)$$

where the parameters ν and θ are given by

$$\nu = \frac{\kappa^2(1)}{\kappa(2)}, \theta = \frac{\kappa(2)}{\kappa(1)}. \quad (21)$$

The accuracy of the Gamma model is illustrated later in simulation results in Fig. 6.

D. WR Thinning with respect to Harvested Power

With the assistance of WRs, it is possible to act on the constraints of path loss in a mmWave network and also extend the communication distance while improving the quality of communication. In this section we characterize the conditions required for a WR aided transmission in mmWave communication networks.

As stated before, some of the WR nodes may not be able to harvest enough energy and as a result they may not be available or capable to aid the transmission from source nodes to the destination node. In such a scenario, only a subset of the WR nodes may participate in the communication, which are termed as active WRs. In this subsection we give an insight on such active WRs. Let ρ be the minimum power required to excite the receiver circuits of the destination. Now, taking into account the path loss during the link r_{RD}, the minimum power required by the WRs for transmission is

$$P_{\mathrm{R}} = \rho\, r_{\mathrm{RD}}^{\alpha_j}. \quad (22)$$

Let the network coverage area of the WRs be denoted by $A \in R^2$. The number of points of Φ_{R} within this area, $\Phi_{\mathrm{R}}(A)$, is a Poisson random variable with intensity $\lambda_{\mathrm{R}} A$. The points of the process $\Phi_{\mathrm{R}} = \{x_1, x_2, x_3, \ldots, x_i, \ldots\}$ represent the set of WR node locations. The fact that some of the WR nodes are not available applies a thinning operation on the original Poisson point process. Thinning of the PPP leads to the well-known Matern Hard-core point process (MPP) that has been used to appropriately model networks with guard zones [34].

Additionally, for mmWave systems, the characterization of hardcore models of point processes needs to take into consideration the fading and blockage environments. In this regard, thinning with respect to fading is considered in [35] and [34], while thinning considering blockages is analyzed in [14]. In this paper, we leverage the results from [14], [34] and incorporate the effects of EH and blockages. The characterization of HCPP models via the Laplace Functional and probability generating functionals is quite difficult to analyze and hasn't been properly done yet. [35]–[37]. However, the nodes further away from the hard core distance, d can still be modeled as a PPP as was shown in [35], [36]. In [37], it was stated that MHCPP type II is better approximated with a PPP rather than Type I. Hence, for analytical tractability, we take into account such an approximation and consider that the distribution of the WRs follows a PPP, and their density is approximated by that of the density of a modified hard-core PPP $\bar{\lambda}_{\mathrm{R}}$.

Let Φ_{R} be the primary point process and $\bar{\Phi}_{\mathrm{R}}$ be the generalized MHCPP. In order to generalize the traditional MHCPP with respect to EH power, the hard-core distance d is replaced with the received SINR[2]. A WR node is retained in $\bar{\Phi}_{\mathrm{R}}$ if and only if it has the lowest mark in its neighborhood set of WRs $N(x_i)$ which is determined by dynamically changing the random-shaped region defined by instantaneous path gains, which can be looked upon as the communication range. Hence, after the thinning, only the WRs with sufficient EH power stay inside the process.

Lemma: Let in the disc N, the retaining probability of a WR node is $\mathcal{P}_{\mathrm{R}} = \frac{1 - e^{-N\mathcal{P}_\zeta}}{N\mathcal{P}_\zeta}$. Then the intensity of active number of WRs is given by $\bar{\lambda}_{\mathrm{R}} = \lambda_{\mathrm{R}} \mathcal{P}_{\mathrm{R}}$ [34, Theorem 4.1].

[2]The received SINR at the receiver depends on the amount of transmitted EH power, which in turn decides if the information is successfully decoded at the destination.

Now, in order to find $\mathcal{P}_{\mathrm{R}}$[3], we have to compute the neighborhood success probability $\mathcal{P}_{\zeta}$. The neighborhood set of any WR is determined by bounding the observation region by $\mathcal{B}_{x_i}(r_d)$, where r_d is a sufficiently large distance, such that the probability for a WR located beyond r_d to become a neighbor of x_i is a very small number, ϱ. Hence,

$$\mathbb{P}\left\{\frac{\rho\, G_l^{\max}\mathcal{X}}{||x_i - x_j||^{\alpha}} > \gamma_{\mathrm{R}} |\, ||x_i - x_j|| > r_d\right\} \leq \varrho, \tag{23}$$

where γ_{R} is the minimum required target SNR.

Hence, r_d can be deterministically computed as

$$r_d = \left(\frac{\rho\, G^{\max}}{\gamma_{\mathrm{R}}} F_{\mathcal{X}}^{-1}(\varrho)\right)^{1/\alpha}, \tag{24}$$

where, F^{-1} denotes the inverse of the CDF of $\mathcal{X}_{\mathcal{N}}$.

Then the neighborhood success probability within the bounded region can be defined as

$$\mathcal{P}_{\zeta} = \mathbb{P}\{\gamma_{x_i,x_j} \geq \gamma_{\mathrm{R}} | x_j \in \mathcal{B}_{x_i}(r_d)\}. \tag{25}$$

Therefore, considering blockages (25) can be written as

$$\begin{aligned}\mathcal{P}_{\zeta} &= \sum_{i\in \mathrm{L,N}} \int_0^{r_d} \left(1 - F_{\mathcal{X}}\left(\frac{\gamma_{\mathrm{R}} r^{\alpha_i}}{\rho\,(G^{\max})^2}\right)\right) p_j(r)\, r \mathrm{d}r, \\ &= \sum_{i\in \mathrm{L,N}} \int_0^{r_d} \left[\gamma\left(m, \frac{(\gamma_{\mathrm{R}} r^{\alpha_i})}{\rho\, G^{\max}}\right)\right] p_j(r)\, r \mathrm{d}r. \end{aligned} \tag{26}$$

where, $\gamma(.)$ is the lower incomplete gamma function. A closed form expression for $\mathcal{P}_{\zeta}$can be evaluated numerically.

Using (26), we can derive the generalized MHCPP process of the WRs and their active nodes which have enough EH power to transmit and withstand the blockage effects in the network to transfer the information with less outage probability.

From the above analysis, it is clear that the achievable capacity of a WR assisted link depends on the distance between the WR and the reference point. Assume that our communication region has a radius r_d, then source-destination pair should select the optimal WR with distance less than r_d. In the subsequent section, we discuss the node isolation probability and coverage probability with respect to the typical destination inside the communication region.

IV. Performance Analysis

Node isolation probability, coverage and connectivity are three important metrics, which have received considerable attention during the last decade in the analysis of ad-hoc cellular networks. Connectivity is an important parameter that WR node is necessarily connected to either the source or destination node. As discussed in the previous section, a WR should have a communication range within which the destination node must be located to decode the forwarded message successfully. Due to wireless medium, some nodes are not connected to their neighbors which are treated as isolated nodes. These performance metrics have been studied in recent literature [6], [14], [38]. Due to the impact of blockages, these parameters can be of paramount importance in the characterization of mmWave systems too. Hence, from the perspective of our system model, we analyze these metrics one at a time below.

[3]For details on finding the active node density, please refer to [14].

A. Isolation Probability

The node isolation probability is defined as the probability that a typical destination is not connected to any of the WR nodes, which also means that typical destination is not in communication range of WRs. Communication range can be defined as the range around the transmitter in which the destination is located and can successfully decode the message. The isolation probability of any WR node is determined by bounding the communication region by $\mathcal{B}_{x_i}(r_d)$, where r_d is a sufficiently large distance.

Now, taking interference and random propagation effects of the network the communication range r_d can be rewritten as

$$r_d = \left(\frac{\sigma^2_{\mathrm{RD}}\gamma_{\mathrm{R}}}{P_{\mathrm{R}}\, G_l^{\max}\mathcal{X}}\left(1 + \sum_{i\in\Phi_{\mathrm{R}}} \rho G_i^{\max}\mathcal{X}_i r_{\mathrm{RD}_i}^{-\alpha_j}\right)\right)^{-1/\alpha}. \tag{27}$$

In practical mmWave networks, the communication range or coverage of network fluctuates randomly due to EH power, presence of severe blockage conditions and interference from other WRs. The aggregate interference is a shot noise process, which sometimes may diverge to infinity, making it impossible to make a connection between a WR and the destination. Therefore, (27) is a function of many random variables and the interference sum needs to be characterized before evaluating the intended range r_d .

Now, the required isolation probability with respect to the given communication range can be defined as the probability that the typical destination node is unable to communicate with any of the WRs. Mathematically, a node x_i is isolated if its best nearest node is located outside its communication range. If the destination's best nearest WR node is at a distance d away, then the destination is isolated if $d > r_d$.

$$\mathbb{P}\left\{d > r_d\right\} = \mathbb{E}_{r_d}\left[e^{-\pi\lambda_{\mathrm{R}} r_d^2}\right]. \tag{28}$$

Proposition 3. *The node isolation probability can be tightly lower bounded by*

$$P_i \geq \left[e^{-\pi\lambda_{\mathrm{R}}\left(\frac{\sigma^2_{\mathrm{RD}}\gamma_{\mathrm{R}}}{P_{\mathrm{R}}\, G_l^{\max}}\right)^{\frac{-2}{\alpha}} \mathbb{E}[\mathcal{X}^{\frac{2}{\alpha}}]\mathbb{E}_{\Phi_{\mathrm{R}}}[\left(1+I_{\Phi_{\mathrm{R}}}\right)^{-2/\alpha}]}\right]. \tag{29}$$

Proof. As mentioned earlier, the communication range r_d is a function of many random variables. Then the node isolation probability (28) can be rewritten using Jensen's inequality as

$$P_i = \mathbb{E}_{r_d}\left[e^{-\pi\lambda_{\mathrm{R}} r_d^2}\right] \geq \left[e^{-\pi\lambda_{\mathrm{R}}\mathbb{E}_{r_d}[r_d^2]}\right], \tag{30}$$

where the expectation is taken over the distribution of communication range. Hence, the expectation over communication range can be computed using (27) as

$$\mathbb{E}[r_d] = \mathbb{E}_{\mathcal{X},\mathrm{L}}\left[\left(\frac{\sigma^2_{\mathrm{RD}}\gamma_{\mathrm{R}}}{\rho\, G_l^{\max}\mathcal{X}}\left(1+\sum_{i\in\Phi_{\mathrm{R}}}\rho G_i^{\max}\mathcal{X}_i r_{\mathrm{RD}_i}^{-\alpha_j}\right)\right)^{-2/\alpha_{\mathrm{L}}}\right] + \mathbb{E}_{\mathcal{X},\mathrm{N}}\left[\left(\frac{\sigma^2_{\mathrm{RD}}\gamma_{\mathrm{R}}}{\rho\, G_l^{\max}\mathcal{X}}\left(1+\sum_{i\in\Phi_{\mathrm{R}}}\rho G_i^{\max}\mathcal{X}_i r_{\mathrm{RD}_i}^{-\alpha_j}\right)\right)^{-2/\alpha_{\mathrm{N}}}\right],$$

$$= \mathbb{E}_{\mathrm{L},\mathcal{X},I_{\Phi_{\mathrm{R}}}}\left[\left(\frac{\sigma^2_{\mathrm{RD}}\gamma_{\mathrm{R}}}{\rho\, G_l^{\max}\mathcal{X}}\left(1+I_{\Phi_{\mathrm{R}}}\right)\right)^{-2/\alpha_{\mathrm{L}}}\right] + \mathbb{E}_{\mathrm{N},\mathcal{X},I_{\Phi_{\mathrm{R}}}}\left[\left(\frac{\sigma^2_{\mathrm{RD}}\gamma_{\mathrm{R}}}{\rho\, G_l^{\max}\mathcal{X}}\left(1+I_{\Phi_{\mathrm{R}}}\right)\right)^{-2/\alpha_{\mathrm{N}}}\right],$$

$$= \left(\frac{\sigma^2_{\mathrm{RD}}\gamma_{\mathrm{R}}}{\rho\, G_l^{\max}}\right)^{\frac{-2}{\alpha_{\mathrm{L}}}}\mathbb{E}[\mathcal{X}^{\frac{2}{\alpha_{\mathrm{L}}}}]\mathbb{E}_{I_{\Phi_{\mathrm{R}}}}[(1+I_{\Phi_{\mathrm{R}}})^{-2/\alpha_{\mathrm{L}}}] + \left(\frac{\sigma^2_{\mathrm{RD}}\gamma_{\mathrm{R}}}{\rho\, G_l^{\max}}\right)^{\frac{-2}{\alpha_{\mathrm{N}}}}\mathbb{E}[\mathcal{X}^{\frac{2}{\alpha_{\mathrm{N}}}}]\mathbb{E}_{I_{\Phi_{\mathrm{R}}}}[(1+I_{\Phi_{\mathrm{R}}})^{-2/\alpha_{\mathrm{N}}}] \quad (31)$$

where the moments of interference can be obtained similar to the cumulant characterization of the EH power in (19) using the following relation between moments and cumulants.

$$\kappa(n) = \mu'_n - \sum_{m=1}^{n-1}\binom{n-1}{m}\kappa_m\mu'_{n-m}, \quad (32)$$

where μ'_n represent the moment.

Alternatively, since $I_{\Phi_{\mathrm{R}}}$ is assumed to follow a gamma random variable with parameters as given in (21), we have

$$\mathbb{E}_{I_{\Phi_{\mathrm{R}}}}[(1+I_{\Phi_{\mathrm{R}}})^{-2/\alpha}] = \sum_{j\in\mathrm{L,N}}\int_0^\infty (1+y)^{\frac{2}{\alpha_j}}\frac{y^{\nu-1}e^{-y/\theta}}{\theta^\nu\Gamma(\nu)}\mathrm{d}y, = \mathrm{K}_U(\nu,\nu+1-\tfrac{2}{\alpha_j},\tfrac{1}{\theta}). \quad (33)$$

where K_U is kummerU function, which is also known as Tricomi function. □

WR Node connectivity: We define the probability of WR node connectivity as the likelihood that any WR–destination pair in the network has at least one path that connects them. It basically gives a measure of the overall connectivity of the mmWave network and is directly related to the node isolation probability of the network. We assume that the radius of the bounded borel r_d is sufficiently large so that the border effects are negligible. Now, the unconditional probability that there are no isolated nodes in the region is given by [39]

$$P_{\mathrm{con}} = \exp(-\pi\bar{\lambda}_{\mathrm{R}} r_d^2 e^{-\pi\bar{\lambda}_{\mathrm{R}}\mathbb{E}[r_d^2]}). \quad (34)$$

The WR Node connectivity can further be related to the coverage probability and looked upon as the number of WRs that cover the destination.

B. WR Selection

We assume that the WRs are selected geographically with respect to the typical destination x_i inside the bounded borel $\mathcal{B}_{x_i}$, as shown in the Fig. 3. We also assume that the WRs inside this borel are connected to a central processing unit so that the channel information of different channels are used to precode the forwarded information. Accordingly, we consider the following two cases: 1) WR to destination link without interference, 2) WR to destination link with interference.

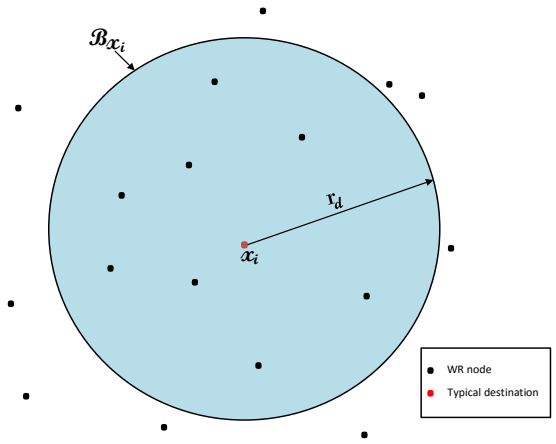

Fig. 3: An illustration of a bounded region of a relay network with respect to the typical destination.

1) WR to destination link without Interference: We assume that the WRs that are located inside $\mathcal{B}_{x_i}$ cooperate among each other, and as a result there is no interference at the destination. The active WRs which can participate in the communication are the ones that are minimally affected by blockages and have a minimum power ρ to transmit. Such a WR with the least path loss can be considered to be the best WR.

Proposition 4. *Let $\gamma \triangleq \frac{\rho G^{\max}}{\sigma^2_{\mathrm{RD}}}$. The CCDF of SNR distribution, $\bar{\gamma}_{\mathrm{RD}}$ of the best WR inside $\mathcal{B}_{x_i}$ can then be given as*

$$\mathcal{P}_{\bar{\gamma}_{\mathrm{RD}}}(T) = \exp\left(-\sum_{j\in\mathrm{L,N}}\frac{1}{\alpha_j}2\pi\lambda\,(\gamma)^{\frac{2}{\alpha_j}} \times \int_t^\infty y^{\frac{-2}{\alpha_j}-1}\int_{y/r_d}^\infty z^{\frac{2}{\alpha_j}} f_{\mathcal{X}}(z)\, e^{-\beta\gamma^{\frac{1}{\alpha_j}}\left(\frac{y}{z}\right)^{-\frac{1}{\alpha_j}}}\mathrm{d}z\mathrm{d}y\right). \quad (35)$$

2) WR to destination link with Interference: The WRs that exist outside $\mathcal{B}_{x_i}$ suffer from interference from each other while forwarding the information. This is due to the assumption that only the ones that are inside the borel know the channel information of each other.

Lemma 1. *The CCDF of SINR distribution of the best WR considering the impact of interference can be given as*

$$\mathcal{P}_{\gamma_{\mathrm{RD}}} = \sum_{k=1}^{m}\binom{m}{k}(-1)^{k+1}\int_1^\infty \exp\left(\frac{-A\,k\,T\,r_{\mathrm{RD}}^{\alpha_{\mathrm{L}}}\sigma^2_{\mathrm{RD}}}{\rho G_l^{\max}}\right) \times \prod_j \mathbb{E}_{I_\Phi^j}\left[\exp\left(\frac{-A\,k\,T r_{\mathrm{RD}}^{\alpha_{\mathrm{L}}} I_\Phi^j}{\rho G_l^{\max}}\right)\right] f_\zeta(r)dr. \quad (36)$$

where f_ζ is the distribution of the nearest WR, which is given by

$$f_\zeta(x) = \lambda(x)e^{-\Lambda(x)}, \tag{37}$$

where $\lambda(x)$ and $\Lambda(x)$ are obtained from Appendix A.

Now, the CCDF of SINR distribution can be given as

$$\begin{aligned}\mathcal{P}_{\gamma_{\mathrm{RD}}} &= \mathbb{P}\left[\frac{\rho G_l^{\max}\,\mathcal{X} r_{\mathrm{RD}}^{-\alpha_{\mathrm{L}}}}{\sigma^2_{\mathrm{RD}} + \sum\limits_{i\in\Phi_{\mathrm{R}}} \rho G_i^{\max}|h_{\mathrm{RD}_i}|^2 r_{\mathrm{RD}_i}^{-\alpha_j}} > T\right], \\ &= \mathbb{P}\left[\mathcal{X} > \frac{T\, r_{\mathrm{RD}}^{\alpha_{\mathrm{L}}}}{\rho G_l^{\max}}\left(\sigma^2_{\mathrm{RD}} + \sum_{i\in\Phi_{\mathrm{R}}} \rho G_i^{\max}\mathcal{X} r_{\mathrm{RD}_i}^{-\alpha_j}\right)\right], \\ &= \mathbb{P}\left[\mathcal{X} > \frac{T\, r_{\mathrm{RD}}^{\alpha_{\mathrm{L}}}}{\rho G_l^{\max}}\left(\sigma^2 + I_{\Phi_{\mathrm{R}}}\right)\right]. \end{aligned} \tag{38}$$

Leveraging the tight upper bound of a Gamma random variable of parameter m as $\mathbb{P}[g < \gamma] < (1 - e^{-A\gamma})^m$ with $A = m(m!)^{\frac{-1}{m}}$, we approximate (38) as

$$\begin{aligned}\mathcal{P}_{\gamma_{\mathrm{RD}}} \;\approx\; & \sum_{k=1}^{m}\binom{m}{k}(-1)^{k+1} \\ & \times\mathbb{E}_{I_\Phi}\left[\exp\left(\frac{-A\,k\,T\,r_{\mathrm{RD}}^{\alpha_{\mathrm{L}}}}{\rho G_l^{\max}}(\sigma^2 + I_{\Phi_{\mathrm{R}}})\right)\right], \end{aligned} \tag{39}$$

where $A = m(m!)^{\Lambda\frac{-1}{m}}$.

Now considering both LOS and NLOS WRs, we have

$$I_\Phi = I_{\Phi_{\mathrm{R}}^{\mathrm{L}}} + I_{\Phi_{\mathrm{R}}^{\mathrm{N}}} \tag{40}$$

Accordingly, we can rewrite (39) as

$$\begin{aligned}\mathcal{P}_{\gamma_{\mathrm{RD}}} = \sum_{k=1}^{m}\binom{m}{k}(-1)^{k+1}\exp\left(\frac{-A\,k\,T\,r_{\mathrm{RD}}^{\alpha_{\mathrm{L}}}\sigma^2_{\mathrm{RD}}}{\rho G_l^{\max}}\right) \\ \times\prod_j \mathbb{E}_{I_\Phi^j}\left[\exp\left(\frac{-A\,k\,T r_{\mathrm{RD}}^{\alpha_{\mathrm{L}}} I_\Phi^j}{\rho G_l^{\max}}\right)\right], \end{aligned} \tag{41}$$

The expectation for the LOS case is given as

$$\begin{aligned}&\mathbb{E}_{I_\Phi^{\mathrm{L}}}\left[\exp\left(\frac{-A\,k\,T r_{\mathrm{RD}}^{\alpha_{\mathrm{L}}} I_\Phi^{\mathrm{L}}}{\rho G_l^{\max}}\right)\right], \\ &= e^{-2\pi\bar{\lambda}_{\mathrm{R}}}\int_1^\infty\left(1 - \frac{1}{\left(1 + \frac{A\,k\,T\,r_{\mathrm{RD}}^{\alpha_{\mathrm{L}}} G_i^{\max}}{m\,G_l^{\max} x^{\alpha_{\mathrm{L}}}}\right)^m}\right) p_{\mathrm{L}}(x)\mathrm{d}(x). \end{aligned} \tag{42}$$

Similarly, the expectation for the NLOS case can be derived. Hence, using the above proposition, we select the best relay from a set of active relays which are obtained as stated in section III.

TABLE I: Simulation Parameters

Notation	Parameter	Values
r_d	Radius of the bounded region	200 meters
λ_s	Density of source nodes	0.0005, 0.001
β	Blockage density	0.01
$G_l^{\max}$	Antenna Gain	18dB
$G_i^{\max}$	Antenna Gain	10dB
α	Path loss exponent	LOS-2, NLOS-4
P	Node transmit power	1 Watt
N_0	Noise power	Thermal noise + 10dB noise figure.

V. Simulation Results

In this section, we validate our system model and also verify the accuracy of the results mentioned in the propositions. In general, the computations are done through Monte Carlo simulations, which are then used to validate the analytical results[4]. We consider the mmW bandwidth of 2 GHz and carrier frequency 73 GHz. Unless stated otherwise, most of the values of the parameters used are inspired from literature mentioned in the references [4], [5]. A few of the parameters and their corresponding values are given in Table I. Every other parameters and values will be explicitly mentioned wherever used.

First we compare the CDF of EH power with different blockage densities for the exponential blockage model in Fig. 4. This result validates proposition 1. It can be seen that the gap between the analytical and simulation results obtained after numerical evaluation of (10) is very tight. It can also be seen from the figure that blockages have considerable impact on the harvesting of power. As we increase the blockage density, the probability of harvested power of a WR for a fixed transmit power reduces.

After establishing the effect of blockages in the previous figure, we now look into the effect path loss exponent α on the EH power. Hence, in the next figure we consider the NLOS case for the fixed blockage model, where the path loss exponent values are greater than 3. Accordingly, in Fig. 5 we compare the CDF of EH power for NLOS case with different path loss exponents. This result validates corollary 2 as the performance gap between the analytical and simulation results is minimal. It is evident from the figure that similar to the effect of blockage densities, higher path loss also reduces the efficiency of EH of the WRs.

Next, we analyze the EH power with respect to the cumulant characterization of the EH power in Fig. 6. The settings for this figure are kept similar to Fig. 4. It can be seen from the figure that the gap between the simulation and cumulant curves is quite small. The cumulant approach for characterizing the EH power can hence be considered as a suitable alternative to the Laplace transform approach. We would like to note that the computational time of Fig. 6 was $1/3$ of the time required to compute Fig. 4.

[4]The parameters considered for simulation in this paper have been taken from recent mmWave studies [3], [5], [9].

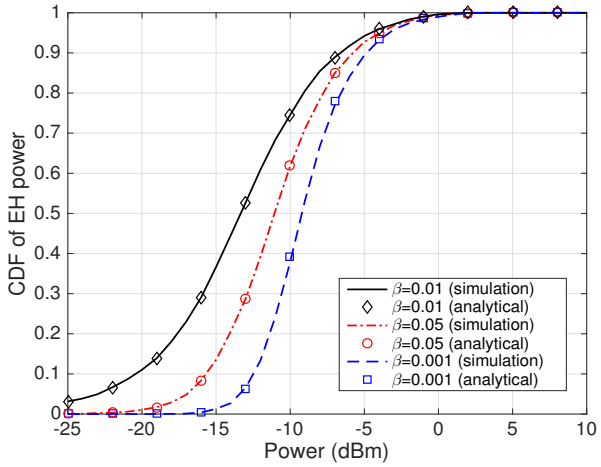

Fig. 4: CDF of the amount of EH power per time slot for different blockage densities.

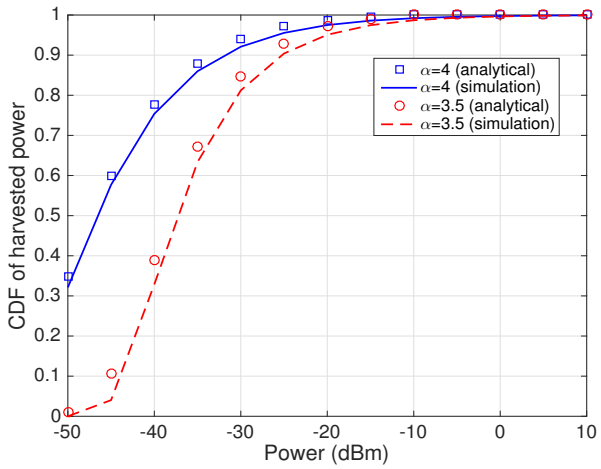

Fig. 5: CDF of the amount of EH power per time slot for different path loss exponents.

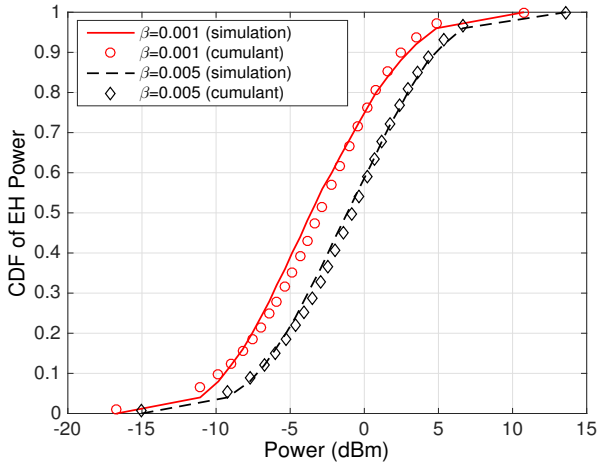

Fig. 6: CDF of the amount of EH power per time slot for different blockage densities (cumulant approach).

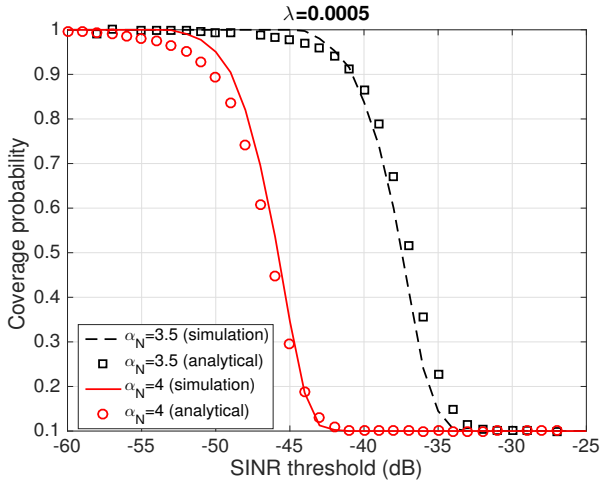

(a) Density of the WRs $\bar{\lambda}_{\mathrm{R}} = 0.0005$

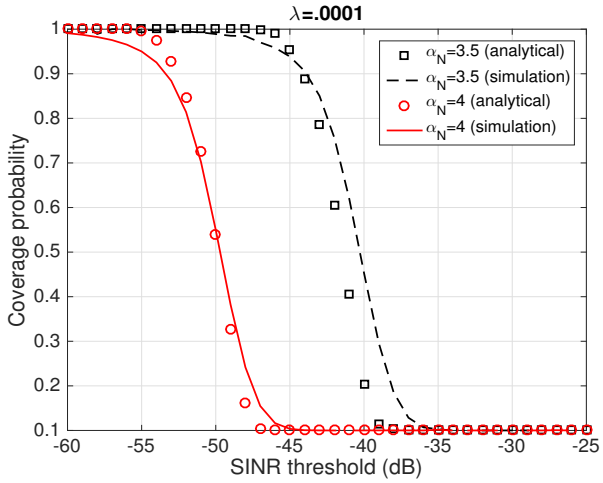

(b) Density of the WRs $\bar{\lambda}_{\mathrm{R}} = 0.0001$

Fig. 7: Coverage probability of the WRs with respect to SINR threshold.

Hereinafter, we focus on the performance analysis of the WRs as was discussed in section IV. Accordingly, in Fig. 7, we show the comparison of the coverage probabilities of the achievable SINR of a relay link under two WR densities. It is evident from both the figures that the coverage probability is higher for smaller values of path loss exponent. It is due to the fact that larger path loss exponent values cause higher path loss in communication. Furthermore, it can be seen from Fig. 7a and Fig. 7b that higher network density leads to a lower coverage probability, which is in contrast to microwave networks. Similar results were also obtained in [4]. We would also like to note that interference becomes negligible with the increase in blockage density. Under such noise limited scenarios, increasing the network density will lead to higher coverage probability.

In Fig. 8, we show the comparison of the coverage probabilities of the achievable SNR for the entire mmWave network aided by a WR. As can be seen from the figure, the increase in density of the WRs under a noise limited scenario improves the coverage probability of the network.

Finally in Fig. 9, we illustrate the effect of WR node density on the WR node connectivity under different r_d values. It can be seen from the figure that WR node connectivity improves, or in other words the number of WRs covering the destination increases for lower values of r_d and decreases for higher r_d. It is also evident from the figure that the density of WRs has a strong impact on the WR node connectivity.

At this point we would like to mention that while powering relays wirelessly is a possibility in a mmWave network, it is heavily dependent on the blockage density and path loss exponent as was seen from Fig. 4, 5, 6. Furthermore, it can be seen from Fig. 7 and 8 that such wirelessly powered relays can be beneficial in increasing the coverage probability of the network. Moreover, blockage density plays a major role in determining the impact of interference of the WRs on the destination.

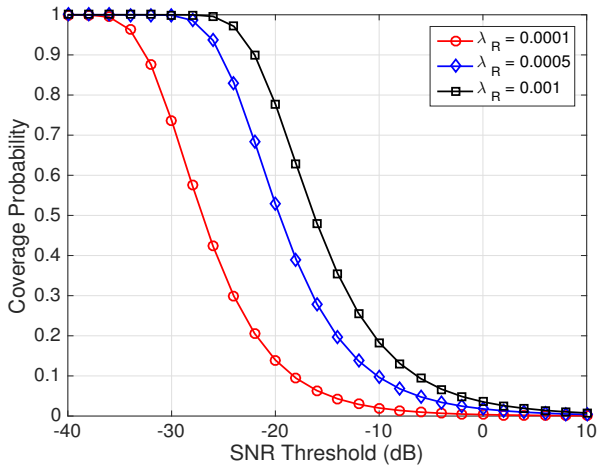

Fig. 8: Coverage probability of the entire network with respect to SNR threshold.

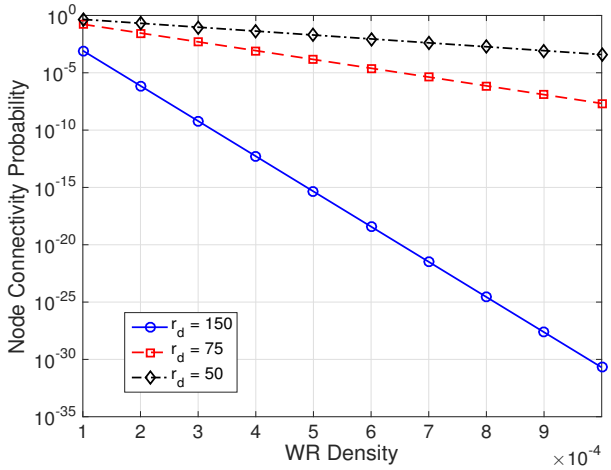

Fig. 9: Node connectivity probability as a function of relay density.

VI. Conclusion

The potential benefits of deploying WRs in outdoor mmWave networks were investigated. From our analysis, it is clear that the achievable harvested energy at a WR depends on the blockage density and network conditions such as path loss exponent, antenna gain, and density of the WRs. In practical scenarios, selecting a relay from an observation (or defined) region with a small neighborhood set of relays is quite optimal. Since the computational complexity increases with the number of relays, a carefully designed region (bounded region) can be taken into consideration. Accordingly, performance metrics, namely coverage, node isolation and network connectivity probabilities for the WRs based on the bounded region were studied. In particular, the coverage probability was analyzed for both within and outside the bounded region.

Appendix A
Proof of Proposition 4

We converge the two dimension relay PPP in planar space into one dimension PPP in line space. Let $\Phi = \left\{x_i = \gamma r_{\mathrm{RD}}^{-\alpha_j}\right\}$ be path gain process, where $j \in \{\mathrm{L},\ \mathrm{N}\}$, $\gamma \triangleq \frac{\rho G^{\max}}{\sigma^2_{\mathrm{RD}}}$. By using Mapping theorem [40], the density function under the effect of blockages can be given as

$$\lambda(x) = \sum_{j\in \mathrm{L,N}} \frac{2\pi\bar{\lambda}_{\mathrm{R}}}{\alpha_i} (\gamma)^{\frac{2}{\alpha_i}}\, x^{\frac{-2}{\alpha_i}-1} f_j(x). \tag{43}$$

where $f_j(x) = e^{-\beta\,\gamma^{\frac{1}{\alpha_j}}\, x^{-\frac{1}{\alpha_j}}}$.

Since our propagation process Φ is also effected by fading conditions, using the displacement theorem [40], the updated density in bounded region can be given as

$$\hat{\lambda}(y) = \int_0^{r_d} \lambda(x)\rho(x,y)\ \mathrm{d}x, \tag{44}$$

where

$$\rho(x,y) = \frac{\mathrm{d}}{\mathrm{dy}}(1 - F_{\mathcal{X}_{\mathcal{N}}}(y/x)) = -\tfrac{y}{x^2} f_{\mathcal{X}_{\mathcal{N}}}(y/x). \tag{45}$$

Thus (44) becomes

$$\begin{aligned}
\hat{\lambda}(y) =& \sum_{j\in \mathrm{L,N}} \frac{1}{\alpha_j} \int_0^{r_d} 2\pi\lambda\,(\gamma)^{\frac{2}{\alpha_i}} x^{\frac{-2}{\alpha_i}-1} \rho(x,y)\, f_j(x)\mathrm{d}x,\\
=& \sum_{j\in \mathrm{L,N}} \frac{1}{\alpha_j} \int_0^{r_d} 2\pi\lambda\,(\gamma)^{\frac{2}{\alpha_i}} x^{\frac{-2}{\alpha_i}-1} f_{\mathcal{X}}(y/x) \tfrac{f_j(x)}{x}\ \mathrm{d}x,\\
\overset{(z=\frac{y}{x})}{=}& \sum_{j\in \mathrm{L,N}} \frac{1}{\alpha_j} 2\pi\lambda\,(\gamma)^{\frac{2}{\alpha_i}} y^{\frac{-2}{\alpha_i}-1} \int_{y/r_d}^{\infty} z^{\frac{2}{\alpha_i}} f_{\mathcal{X}}(z)\, f_j(y/z)\mathrm{d}z.
\end{aligned}$$

Using the void probability of a PPP, the path gain distribution for best relay in interval of (t,∞) can thus be given as

$$\begin{aligned}
\mathcal{P}_{\bar{\gamma}_{\mathrm{RD}}}(T) &= \exp\left(-\int_t^{\infty} \hat{\lambda}(y)\mathrm{d}y\right)\\
&= \exp\left(-\sum_{j\in \mathrm{L,N}} \frac{1}{\alpha_i} 2\pi\lambda\,(\gamma)^{\frac{2}{\alpha_j}} \right.\\
&\qquad \left. \times \int_t^{\infty} y^{\frac{-2}{\alpha_j}-1} \int_{y/r_d}^{\infty} z^{\frac{2}{\alpha_j}} f_{\mathcal{X}}(z)\, f_j(y/z)\mathrm{d}z\mathrm{d}y\right).
\end{aligned} \tag{46}$$

REFERENCES

[1] S. Biswas, C. Masouros, and T. Ratnarajah, "Performance analysis of large multi-user mimo systems with space-constrained 2d antenna arrays," *IEEE Trans. on Wireless Communications*, vol. PP, no. 99, pp. 1–1, 2016.

[2] A. Ghosh, T. Thomas, M. Cudak, R. Ratasuk, P. Moorut, F. Vook, T. Rappaport, G. Maccartney, S. Sun, and S. Nie, "Millimeter-wave enhanced local area systems: A high-data-rate approach for future wireless networks," *IEEE Journal on Selected Areas in Communications*, vol. 32, no. 6, pp. 1152–1163, June 2014.

[3] A. Ghosh, T. N. Thomas, M. C. Cudak, R. Ratasuk, P. Moorut, F. W. Vook, T. S. Rappaport, G. R. MacCartney, S. Shun, and S. Nie, "Millimeter-wave enhanced local area systems: A high data-rate approach for future wireless networks," *IEEE J. Select. Areas Commun.*, vol. 32, no. 6, pp. 1153–1163, June 2014.

[4] A. Thornburg, T. Bai, and R. W. Heath, "Performance analysis of mmWave ad hoc networks," can be found at http://arxiv.org/abs/1412.0765, 2016.

[5] S. Singh, M. N. Kulkarni, A. Ghosh, and J. G. Andrews, "Tractable model for rate in self-backhauled millimeter wave cellular networks," *IEEE J. Select. Areas Commun.*, vol. 33, no. 1, pp. 2196–2211, Jan. 2015.

[6] T. A. Khan, A. Alkhateeb, and R. W. H. Jr., "Millimeter wave energy harvesting," *CoRR*, vol. abs/1509.01653, 2015. [Online]. Available: http://arxiv.org/abs/1509.01653

[7] B. Medepally and N. Mehta, "Voluntary cooperative energy harvesting relay nodes: Analysis and benefits," in *Proc. IEEE International Conference on Communication (ICC'2010)*, Cape Town, SA., May23-27 2010, pp. 1 – 6.

[8] M. Akdeniz, Y. Liu, S. Rangan, and E. Erkip, "Millimeter wave picocellular system evaluation for urban deployments," in *Proc. IEEE Global Telecommunications Conference (Globecom'13)*, Dec. 2013, pp. 105–110.

[9] M. R. Akdeniz, Y. Liu, M. K. Samimi, S. Shun, S. Rangan, T. S. Rappaport, and E. Erkip, "Millimeter-wave channel modeling and cellular capacity evaluation," *IEEE J. Select. Areas Commun.*, vol. 32, no. 6, pp. 1164–1179, June 2014.

[10] S. Rajagopal, S. Abu-Surra, and M. Malmrichegini, "Channel feasibility for outdoor non-line-of-sight mmWave mobile communication," in *Proc. IEEE Vehicular Technology Conference (VTC'12 Fall)*, 2012, pp. 1–6.

[11] J. N. Laneman, D. N. C. Tse, and G. W. Wornell, "Cooperative diversity in wireless networks: Efficient protocols and outage behavior," *IEEE Trans. Inform. Theory.*, vol. 50, no. 12, pp. 3062–3080, 2004.

[12] M. Renzo, F. Graziosi, and F. Santucci, "A comprehensive framework for performance analysis of dual-hop cooperative wireless systems with fixed-gain relays over generalized fading channels," *IEEE Trans. Wireless Commun.*, vol. 8, no. 10, pp. 5060–5074, Oct. 2009.

[13] S. W. Peters, A. Y. Panah, K. T. Truong, and R. W. Heath, "Relay architectures for 3GPP LTE-advanced," *EURASIP Journal on Wireless Communications and Networking*, p. 14pages, Jul. 2009.

[14] S. Biswas, S. Vuppala, J. Xue, and T. Ratnarajah, "On the performance of relay aided millimeter wave networks," *IEEE Journal of Selected Topics in Signal Processing*, vol. PP, no. 99, pp. 1–1, 2015.

[15] M. D. Renzo and W. Lu, "End-to-end error probability and diversity analysis of AF-based dual-hop cooperative relaying in a Poisson field of interferers at the destination," *IEEE Trans. Wireless Comm.*, vol. 4, no. 1, pp. 15 – 32, Jan. 2015.

[16] A. Behnad, A. M. Rabiei, and N. C. Beaulieu, "Performance analysis of opportunistic relaying in a Poisson field of amplify-and-forward relays," *IEEE Trans. Communications.*, vol. 61, no. 1, pp. 97–107, Jan. 2013.

[17] W. Lu and M. D. Renzo, "Performance analysis of relay aided cellular networks by using stochastic geometry," in *Proc. IEEE* 19^th *International Workshop on Computer Aided Modeling and Design of Communication Links and Networks*, Athens, Greece, Dec.

[18] Z. Lin, Y. Gao, X. Zhang, and D. Yang, "Stochastic geometry analysis of achievable transmission capacity for relay-assisted device-to-device networks," in *Proc. IEEE International Conference on Communications - Mobile nad Wireless Networking Symposium*, Sydney, Austrlia, June 2014.

[19] Z. Lin, X. Peng, F. Chin, and W. Feng, "Outage performance of relaying with directional antennas in the presence of co-channel interferences at relays," *IEEE Wireless Communicatin Letters*, vol. 1, no. 4, pp. 288 – 291, Aug. 2012.

[20] D. Michalopoulos and G. Karagiannidis, "Phy-layer fairness in amplify and forward cooperative diversity systems," *IEEE Transactions on Wireless Communications*, vol. 7, no. 3, pp. 1073–1082, March 2008.

[21] T. Himsoon, W. Siriwongpairat, Z. Han, and K. Liu, "Lifetime maximization via cooperative nodes and relay deployment in wireless networks," *IEEE Journal on Selected Areas in Communications*, vol. 25, no. 2, pp. 306–317, February 2007.

[22] H. ElSawy, E. Hossain, and M. Haenggi, "Stochastic geometry for modeling, analysis, and design of multi-tier and congnitive cellular wireless networks: A survey," *IEEE Communications Surveys and Tutorials*, vol. 15, no. 3, pp. 996 – 1019, July 2013.

[23] J. G. Andrews, F. Baccelli, and R. K. Ganti, "A tractable approach to coverage and rate in cellular networks," *IEEE Trans. Commun.*, vol. 59, no. 11, pp. 3122–3134, Nov. 2011.

[24] S. Akoum, E. O. Ayach, and R. W. Heath, "Coverage and capacity in mmWave cellular systems," in *Proc. IEEE Asilomar Conference on Signals, Systems and Computers*, 2012, pp. 688–692.

[25] T. Bai, R. Vaze, and R. W. Heath, "Analysis of blockage effects on urban cellular networks," *IEEE Trans. Wireless Comm.*, vol. 13, no. 9, pp. 5070–5083, June 2014.

[26] Z. Yi and I.-M. Kim, "Optimum beamforming in the broadcasting phase of bidirectional cooperative communication with multiple decode-and-forward relays," *IEEE Transactions on Wireless Communications*, vol. 8, no. 12, pp. 5806–5812, December 2009.

[27] H.-M. Kim, T.-K. Kim, M. Min, and G.-H. Im, "Low-complexity detection scheme for cooperative mimo systems with decode-and-forward relays," *IEEE Transactions on Communications*, vol. 63, no. 1, pp. 94–106, Jan 2015.

[28] M. Haenggi, "A geometric interpretation of fading in wireless networks: Theory and applications," *IEEE Trans. Inform. Theory*, vol. 54, no. 12, pp. 5500 – 5510, Dec. 2008.

[29] T. Bai and R. W. Heath, "Coverage and rate analysis for millimeter-wave cellular networks," *IEEE Trans. Wireless Commun.*, vol. 14, no. 2, pp. 1100–1114, Feb. 2015.

[30] A. Sakr and E. Hossain, "Analysis of k -tier uplink cellular networks with ambient rf energy harvesting," *IEEE Journal on Selected Areas in Communications*, vol. 33, no. 10, pp. 2226–2238, Oct 2015.

[31] J. Evans and D. Everitt, "On the teletraffic capacity of cdma cellular networks," *IEEE Transactions on Vehicular Technology*, vol. 48, no. 1, pp. 153–165, Jan 1999.

[32] C. Lam and T. LE-NGOC, "Log-shifted gamma approximation to log-normal sum distributions," *IEEE Transactions on Vehicular Technology*, vol. 56, no. 4, pp. 2121–2129, July 2007.

[33] A. Ghasemi and E. S. Sousa, "Interference aggregation in spectrum-sensing cognitive wireless networks," *IEEE Journal on Selected topics in Signal Processing.*, vol. 2, no. 1, pp. 41 – 56, Feb. 2008.

[34] H. ElSawy and E. Hossain, "A modified hard core point process for analysis of random CSMA wireless networks in general fading environments," *IEEE Trans. Commun.*, vol. 61, no. 4, pp. 1520 – 1534, April 2013.

[35] H. Q. Nguyen, F. Baccelli, and D. Kofman, "A stochastic geometry analysis of dense IEEE 802.11 networks," in *IEEE International International Conference on Computer Communications*, 2007, p. 11991207.

[36] A. Hasan and J. G. Andrews, "The guard zone in wireless ad hoc networks," *IEEE Trans. Wireless Comm.*, vol. 4, no. 3, pp. 897–906, March 2007.

[37] M. Haenggi, "Mean interference in hard-core wireless networks," *IEEE Commun. Lett.*, vol. 15, no. 8, pp. 792–794, Aug. 2011.

[38] D. Miorandi, "The impact of channel randomness on coverage and connectivity of ad hoc and sensor networks," *IEEE Transactions on Wireless Communications*, vol. 7, no. 3, pp. 1062–1072, March 2008.

[39] C. Bettstetter and C. Hartmann, "Connectivity of wireless multihop networks in a shadow fading environment (2005):," *Wireless Networks*, pp. 571–579, Sept. 2005.

[40] M. Haenggi, *Stochastic Geometry for Wireless Networks*. Cambridge University Press, 2012.